JAMES | Journal of Advances in Modeling Earth Systems

RESEARCH ARTICLE
10.1029/2024MS004369

Tipping to an Aggregated State by Mesoscale Convective Systems

I. L. Kruse[1,2,3], **R. Fiévet**[4], **and J. O. Haerter**[5,6]

[1]Niels Bohr Institute, University of Copenhagen, Copenhagen, Denmark, [2]Leibniz Centre for Tropical Marine Research, Bremen, Germany, [3]Now at: Danish Meteorological Institute, Copenhagen, Denmark, [4]Max Planck Institute for Meteorology, Hamburg, Germany, [5]Physics and Earth Sciences, Constructor University Bremen, Bremen, Germany, [6]Department of Physics and Astronomy, University of Potsdam, Potsdam, Germany

Key Points:

- Tropical MCSs over land, transitioning to sea, are simulated in a CRM by imposing and removing the diurnal cycle in surface temperatures
- Self-aggregation can arise in the otherwise non-aggregating ocean simulations, thanks to the tipping-inducing processes of MCSs over land
- A discrete reaction-diffusion-type conceptual model including boundary layer processes such as cold pools can capture this bi-stability

Correspondence to:
I. L. Kruse,
ikr@dmi.dk

Citation:
Kruse, I. L., Fiévet, R., & Haerter, J. O. (2025). Tipping to an aggregated state by mesoscale convective systems. *Journal of Advances in Modeling Earth Systems*, *17*, e2024MS004369. https://doi.org/10.1029/2024MS004369

Received 29 MAR 2024
Accepted 23 FEB 2025

Author Contributions:
Conceptualization: I. L. Kruse, R. Fiévet, J. O. Haerter
Data curation: I. L. Kruse
Formal analysis: I. L. Kruse
Funding acquisition: J. O. Haerter
Investigation: I. L. Kruse, R. Fiévet, J. O. Haerter
Methodology: I. L. Kruse, J. O. Haerter
Project administration: J. O. Haerter
Resources: J. O. Haerter
Software: I. L. Kruse, R. Fiévet
Supervision: R. Fiévet, J. O. Haerter
Validation: I. L. Kruse
Visualization: I. L. Kruse
Writing – original draft: I. L. Kruse, R. Fiévet, J. O. Haerter
Writing – review & editing: I. L. Kruse, R. Fiévet, J. O. Haerter

Abstract Radiative-convective equilibrium simulations were suggested to resist self-aggregation within a linearly stable regime at low surface temperatures. Recent numerical work shows that this linearly stable regime can rapidly transition to an aggregated state when exposed to realistic diurnal surface temperature variations. The resultant aggregated state is then stable, even when the surface temperature is set constant. Here we argue, by constructing a reaction-diffusion model, that this tipping process can be explained by the formation of mesoscale convective systems under the diurnal forcing. The model implies that strong cold pool interactions, invoked by the diurnal cycle, drive the self-organization of long-term buoyancy memory. Thus, whereas previous conceptual work disregarded the boundary layer dynamics, we here attribute key organizing mechanisms to them: namely the ability to cause rapid self-aggregation over continents and its advection over the ocean—with potential implications for hurricane formation.

Plain Language Summary In simulations that mimic the atmosphere over tropical ocean surfaces with constant temperature, thunderstorms can spontaneously group together, forming large cloud patches surrounded by clear areas. This clustering tends to happen when the ocean surface is warm enough; otherwise, the thunderstorms remain scattered. Recent simulations show that clustering can occur at lower temperatures, if there's a day-to-night temperature oscillation, similar to what happens over land. Once the clustering happens, it can persist even without temperature oscillation. This study proposes a new simplified model that explains this phenomenon by considering interactions between thunderstorms, particularly through "cold pools", dense air caused by rain evaporating under existing precipitating clouds. Previous models did not account for these near-surface effects: Our findings suggest that these interactions are key to understanding cloud clustering. Linking simulations to reality, this insight could have implications for understanding hurricane formation, which could be regarded in this context as cloud clustering starting over tropical African land and intensifying over the Atlantic Ocean.

1. Introduction

In Earth's atmosphere, convection can organize across many spatial scales, from local thunderstorms, to mesoscale convective systems (MCSs), tropical cyclones, and synoptic-scale waves. MCSs are organized clusters of thunderstorms spanning more than 100 km horizontally, persisting often for multiple hours (Houze, 2018). They are known to be the dominant source of rainfall in the tropics (Nesbitt et al., 2000), and the longest-lived MCSs are shown to be largely responsible for tropical extreme precipitation (Roca & Fiolleau, 2020; Tan et al., 2015). Globally, the most extreme storms tend to be located over land, and the most intense storms over oceans tend to be adjacent to land, where motion is favored from land to ocean, for example, tropical West Africa and the adjacent Eastern Atlantic Ocean (Fang & Du, 2022; Zipser et al., 2006). However, the fundamental mechanisms driving the formation, intensification and dissipation of MCSs is not well established yet.

In an effort to better-understand the physics of convective storms, the atmospheric modeling community has been focusing for many years on the concept of Convective Self-Aggregation (CSA). Most cloud-resolving model (CRM) simulations run under radiative convective equilibrium (RCE) adopt a highly idealized modeling setup, typically assuming homogeneous initial and boundary conditions, a constant sea surface temperature (SST), and constant insolation. Under these conditions, convection can spontaneously clump, or aggregate, into domain-wide patterns of persistent dry areas and confined rainy areas over a time-scale of weeks to months (Emanuel et al., 2014; Held et al., 1993; C. Muller et al., 2022; Tompkins & Craig, 1998). CSA, albeit still a modeling

paradigm, could reveal the mechanisms behind some of the convective organization observed in the tropics (Holloway et al., 2017). The process of forming domain-wide structure can be achieved within few days by imposing temporally oscillating surface temperatures with a large enough amplitude (Haerter et al., 2020). The "diurnally aggregated" cloud field is similar to CSA as it also constrains the surface rain field to certain parts of the domain. In fact, in the simulations by Haerter et al. (2020) mesoscale organization vanished when the diurnal cycle was removed. The idealized tropical atmosphere, simulated under RCE conditions with constant SST, is known to exhibit hysteresis effects (Khairoutdinov & Emanuel, 2010; C. J. Muller & Held, 2012). Recent work however describes an alternative route to hysteresis in self-aggregation: under diurnally varying surface temperature forcing, multi-day spatio-temporally persistent dry patches can form. These first initiate in the uppermost atmospheric layers and subsequently penetrate through to the subcloud layer. When removing the diurnal forcing after a number of days, the persistently dry patches remain and are reminiscent of a classical aggregated state (Jensen et al., 2022).

Much uncertainty remains regarding CSA, and a useful tool to further investigate the mechanisms driving it is offered by conceptual models (Biagioli & Tompkins, 2023; Emanuel et al., 2014; Nissen & Haerter, 2021). Emanuel et al. (2014) explore CSA as a linear instability of the homogeneous RCE state of the tropical atmosphere, focusing on clear-sky longwave effects and the role of free-tropospheric moisture, thus neglecting boundary-layer processes. In contrast, Haerter et al. (2020) and Nissen and Haerter (2021) emphasize the role of convective cold pools (CPs) in CSA emergence, with CP collisions driving phase separation akin to CSA formation. In Yanase et al. (2020), the interplay between CPs and radiatively driven dry pools in promoting or inhibiting CSA is investigated, highlighting the importance of the domain size. More recently, Biagioli and Tompkins (2023) build on Craig and Mack (2013) to simulate convective organization, proposing the horizontal transport efficiency of moisture and subsidence rate as key parameters determining an "area of influence" of convection on the vapor field, characterized by a moisture halo surrounding convective updrafts. Importantly, their model can estimate how a specific domain size and resolution is prone to aggregate, at least for constant surface temperatures. While the models above offer valuable insights, they individually overlook key aspects, lack the possibility to resolve both land and sea configurations, disregard boundary layer dynamics, or the integration of CPs contributing as both a negative feedback inside rain cells, that is, the suppression of new convection as a result of cold, dry air injected into the boundary layer; and the positive feedback in their immediate surroundings, that is, the triggering of new convection on the edges of a CP due to mechanical and thermodynamic lifting of the environmental air (Rotunno et al., 1988; Tompkins, 2001; Torri et al., 2015). Together, these simplifications point to the need of a conceptual model that integrates both vertical and horizontal dynamics influencing CSA, valid in different environments.

In this work we aim to strengthen the bridge between the modeling paradigm of CSA and the real atmosphere. Specifically, we build upon the reasoning of Jensen et al. (2022) that if an organized convective cloud field, produced under a high-amplitude surface temperature forcing, is eventually advected over regions with little surface temperature variation, the clustered pattern may persist and even intensify further. In the real atmosphere, the spatio-temporal scales of this phenomenon can be found over the tropical African continent and the adjacent Atlantic Ocean. There, land-born mesoscale convection is advected over the ocean, at times even maturing to tropical cyclones when reaching higher latitudes and thus acquiring rotation. Hereby, we explore how diurnal surface temperature amplitudes, typical of tropical land, affect the formation of persistent dry patches and the spatio-temporal extent of the emergent MCSs.

To this end, we run a set of cloud resolving simulations initialized with typical tropical profiles of temperature and humidity. A large-amplitude diurnally oscillating surface temperature is imposed, which is then set to constant at different times, to see the effect on the diurnally aggregated cloud field. By tracking observed MCSs over West Africa and the adjacent Atlantic, we first show that our simulations give realistic deep convective diurnal cycles under the imposed surface temperature conditions. Analogous to Jensen et al. (2022), persistent mesoscale organization arises in the simulations performed over "land" after running them for several days. When switching to constant surface temperatures, we find strong dependence on the degree of aggregation over "land," in determining its persistence over "sea," thus implicating a form of hysteresis. We capture this hysteresis by deriving a simplified conceptual model. Our model discretizes the boundary layer using a spatial grid scale corresponding to that of typical CPs and captures basics of convective dynamics, radiative effects and CP interaction, both under diurnal and constant-temperature surface conditions.

Table 1
Summary of Simulations

Case name	L_x [km]	L_y [km]	Δx [km]	Duration [days]	T_0 [K]	ΔT [K]	Start time [day]
DIU	480	480	1	56	305	10	0
OCEAN	480	480	1	42	300	0	0
DIU hires	480	480	0.5	28	305	10	0
DIU lores	480	480	4	28	305	10	0
OCEAN hires	480	480	0.5	28	300	0	0
OCEAN lores	480	480	4	28	300	0	0
OCEAN warm	480	480	1	28	305	0	0
branches:							
DIU2OCEAN A_1	480	480	1	28	300	0	DIU 13.25
DIU2OCEAN B_1	480	480	1	28	300	0	DIU 13.5
DIU2OCEAN C_1	480	480	1	28	300	0	DIU 13.75
DIU2OCEAN D_1	480	480	1	28	300	0	DIU 14
DIU2OCEAN A_2	480	480	1	42	300	0	DIU 27.25
DIU2OCEAN B_2	480	480	1	42	300	0	DIU 27.5
DIU2OCEAN C_2	480	480	1	42	300	0	DIU 27.75
DIU2OCEAN D_2	480	480	1	42	300	0	DIU 28

Note. Table 1 indicates the horizontal domain sizes L_x and L_y, the horizontal grid resolution Δx, the duration of each simulation, as well as the imposed surface temperature T_0 and its diurnal amplitude ΔT. We also provide the start time of each simulation. For the branch cases, the initial condition is the state of DIU at the start time specified.

The paper is organized as follows. Section 2 has two parts which each encompass methods and relevant results: in Section 2.1 we introduce the numerical model used to simulate MCSs over tropical Africa and the adjacent Atlantic Ocean and observational data set used to calibrate and validate the former; subsequently we introduce the methods to study self-aggregation and show the emergence of bi-stability in the transition from land to sea; In Section 2.2 we introduce the conceptual model that can capture the bi-stability in self-aggregation from land to sea and its parameter space. In Section 3 we discuss the implications of our results.

2. Methods and Results

2.1. Idealized Simulations of Organized Convection

2.1.1. Numerical Methods

Our numerical simulations (Table 1) are conducted using the System for Atmospheric Modeling, version 6.11 (Khairoutdinov & Randall, 2003). The model uses a single-moment microphysics scheme, the RRTM radiation scheme and a 1.5-order sub-grid scale closure scheme for subgrid turbulent processes. Surface fluxes are evaluated based on the Monin-Obukhov similarity. The computational domain consists of 480 × 480 grid points in the horizontal, with doubly periodic lateral boundary conditions, and a horizontal resolution of 1 km, respectively 500 m for the high-resolution simulations. We use 64 levels in the vertical, with a logarithmic scaling stretching from 50 m at the lowest level to 1,000 m at the top of the model domain, which is set at 27 km and has a sponge layer above. We do not account for Coriolis forces. The vertical profiles are initialized using a tropical sounding without horizontal wind derived from ERA5 data set, averaged over the Atlantic and tropical West Africa (5:10N,−40:10E) in the months of June–August 2020. For all "ocean" simulations (OCEAN), constant surface temperatures $T_s(t) = T_0 = const$ conditions are prescribed domain-wide. As is appropriate for a water surface, the specific humidity at the surface is assumed to be at saturation. For "land" simulations (DIU), we impose sinusoidally-oscillating surface temperatures $T_s(t)$, that is:

$$T_s(t) = T_0 - \Delta T \cos(2\pi t/t_0), \quad (1)$$

where T_0 is the average surface temperature, ΔT is the surface temperature amplitude and $t_0 = 24\ h$ is the one-day period. For DIU, surface latent heat fluxes are reduced to 0.7 of those obtained for the (saturated) oceanic surface, in an effort to mimic an unsaturated surface and to keep the Bowen ratio from becoming too unrealistically low. The temporally-averaged Bowen ratio in the DIU simulation is 0.2 with this "land" set-up, and 0.1 for the OCEAN simulation. These Bowen ratios, calculated from the time-averaged latent heat flux and sensible heat flux over the whole simulations, are approximately representative of tropical rain forest and tropical ocean, respectively (Oliver, 2005).

Finally, as this study focuses on the effects surface temperature variation have on CSA, we remove the top-of-the-atmosphere radiative cycle. It is set to a constant average incoming radiation calculated from July 1st, at 10° North.

2.1.2. Observational Analysis

In an effort to design realistic tropical conditions for our idealized simulations, we first scrutinize satellite imagery over tropical continental Africa, where MCSs are systematically formed over land and advected over the adjacent Atlantic Ocean. In the month of July, which coincides with the beginning of the local monsoon season as well as the Atlantic hurricane season, there is a peak of MCS activity between the latitudes of 0 and 20° N, meaning the MCSs caught in the African Easterly Jet have the longest possible travel time over land. To obtain information on the environment that MCSs are embedded within, in their transition from tropical African land to the adjacent ocean, we use a 5 years-long database of MCSs tracked from geostationary infrared satellite observations (TOOCAN, Fiolleau & Roca, 2013). In Figure 1a, we show the area of interest along with TOOCAN-tracked MCS cloud shields on 14 July 2016. The evolution of groups of MCSs is followed using a Lagrangian frame.

To do this, we place a 15 × 15 degree frame at the time of maximum convective activity of the Eulerian frame (18UTC), that is in the same initial location over tropical West Africa (10:25 N, 6:21 E) as shown in Figure 1a. Then, we follow the movement of the tracked MCSs for every day in July for the 5 years of available TOOCAN data (2012–2016). The frame moves along with the average movement of the areal centers of mass of all the MCSs contained within it. When there are no MCS cloud shields present in the frame, for example, as is common at night over land, the frame continues moving with the average velocity of the previous 3 time steps. The velocity vector of the frame is approximately always westward and the latitudinal component near-zero. While the frame is fully over land, we classify it in the land regime, while if it is partially over land and partially over the ocean, we classify it as a transition regime. Once the frame is fully over the ocean, we classify it as in the ocean regime. We keep tracking the MCSs in the frame, until the left edge of the frame reaches the longitude line of 40 W. We find that the average westward velocity is larger in magnitude when the frame is over land, compared to when it is over the ocean (Figure 1b). The mean longitudinal velocities of the frame while it is over land is -2.8 m s^{-1}, and -1.7 m s^{-1} while it is fully over the ocean. Within the Lagrangian frame tracks, we record domain-averaged values of skin temperature, using ERA5 reanalysis data, along with the TOOCAN MCS fraction within the box. We superimpose all the tracks, take diurnal composites of these, of which we plot the 24 hr timeseries showing the first diurnal cycle from midnight to midnight over land and then over ocean, in 1c. From the Lagrangian tracks, we find a clear diurnal cycle in the frame-averaged skin temperature over land. It has an amplitude of approximately 10 K and oscillates from 295 to 315 K. Conversely, the MCS cover over land exhibits a clear diurnal cycle that lags behind the skin temperature diurnal cycle. Over the ocean, the frame-averaged temperature is constant at approximately 300 K. Compared to land, the MCS cover over the ocean is relatively low and does not exhibit a clear diurnal cycle. We note that the composites are calculated within a moving box, that moves toward the West, that is, with the sun. This means that the diurnal cycles shown in Figure 1c have a slightly longer period than 24 hr.

2.1.3. Comparison Between Observational and Numerical MCSs

We then seek to reproduce the observational findings in Figure 1c (dotted lines) using our idealized CRM output, calibrated with the aforementioned surface temperature time-varying conditions. To this end we calculate composite of consecutive one-day time series of the simulated variables.

In Figure 1c, first row, we see the imposed surface temperatures for the DIU and OCEAN simulations, mimicking best the observations, and consequently the high cloud fraction, a model-produced field which should be

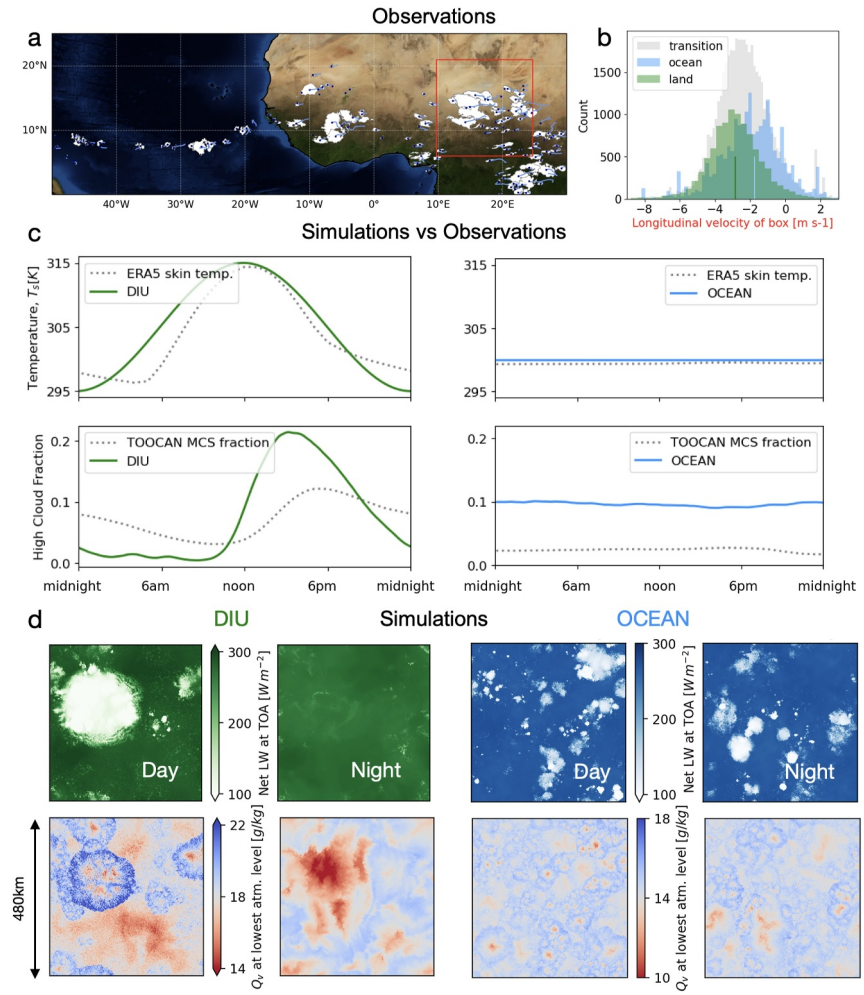

Figure 1. Mimicking realistic diurnal cycle dynamics with idealized cloud resolving simulations. (a) Satellite-observed mesoscale convective systems (MCSs) over tropical Africa (white areas) and 15 × 15 degree Lagrangian frame (thin red square); (b) Longitudinal velocity of Lagrangian frame when over land, ocean, and in the transition zone. The mean values of the ocean and land velocity distributions are indicated by the small vertical lines. (c) Imposed surface temperatures, and domain mean high cloud fraction. The latter is calculated within the simulation domain of DIU and OCEAN respectively. Dotted lines show domain-mean skin temperature (from ERA5 reanalysis) and MCS cover (from TOOCAN tracked MCSs), calculated within the Lagrangian frame that follows tracked MCSs across tropical African land and onto the adjacent Atlantic Ocean, in July 2012–2016. (d) Representative instantaneous horizontal plots of outgoing longwave radiation, OLR, and near-surface specific humidity, Q_v for DIU and OCEAN, as labeled.

compared with the TOOCAN MCS cover. In our idealized simulations, we do capture the diurnal cycle in deep convection seen over land, and a nearly constant deep convective time series over the ocean. However, the high cloud fraction in our simulations nearly reaches zero during the night hours, while MCSs on average persist through the night in the observations, likely aided by realistic phenomena such as wind shear which are not included in our idealized simulations. Furthermore, we note that the modeled high cloud cover over the ocean, is systematically higher than the TOOCAN MCS cover over the ocean. This can be explained by the fact that the "high cloud cover" output of the model includes all high clouds, and there is an abundance of high clouds that wouldn't be defined as MCSs due to their limited extent or optical thickness. When investigating the other variables in the simulations, two striking differences are noticeable between DIU and OCEAN: (a) The patterns of the deep convective clouds and (b) their footprint in the CP field. In DIU, in the convective window of the afternoon, large organized deep convective structures appear that can easily take up a quarter of the domain, reaching sizes of MCSs (Figure 1d). Below these MCS structures large CPs are present—that is, cold patches of air with dry interiors and moist borders, as seen in the near surface specific humidity field in Figure 1d. These

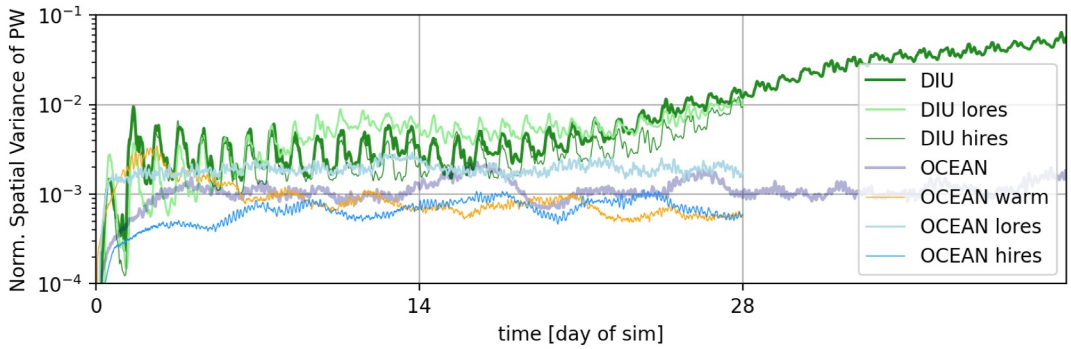

Figure 2. Emerging self-aggregation of convection. Normalized spatial variance Equation 2 of precipitable water (PW) for the cloud-resolving simulation results using the System for Atmospheric Modeling (SAM) as described in Table 1. Note that the DIU simulations (green curves) consistently show a systematic increase in PW over time whereas OCEAN (all other curves) consistently fluctuates around a state of low PW. As indicated in the legend, the simulations explore the sensitivity to numerical model grid resolution and sea surface temperature in the case of OCEAN. Note the logarithmic vertical axis scaling.

cloud structures disappear at night in the outgoing longwave radiation field, but persist in the moisture field as dry patches. In the OCEAN simulations, on the other hand, the deep convection remains relatively small and sparse around the domain, and there is no notion of "day" and "night." Finally, the collocated CPs are also more homogeneous.

2.1.4. Convective Self-Aggregation and Bistability

Further, we investigate the emergence of self-aggregation of convection in our suite of simulations. Similar to previous measures (Wing et al., 2017) we use the normalized spatial variance of precipitable water (PW),

$$\mathrm{Var}(PW) \equiv \langle (PW - \langle PW \rangle)^2 \rangle / \langle PW \rangle^2, \tag{2}$$

as a measure of aggregation of the moisture field. The pointed parentheses here indicate an average over all horizontal grid cells. The normalization ensures that overall changes in moisture do not appear as changes in variance. High values of Var(PW) reflect a more aggregated field, since aggregated convection is characterized by the striking segregation of moist, strongly convecting regions embedded within an otherwise very dry and non-precipitating domain.

We calculate Var(PW) in each time step for all our simulations (Table 1). In the first 14 days of simulation the main difference between DIU and OCEAN (Figure 3) is that DIU shows a large day-to-night variation, with peaks in Var(PW) during the day, when the MCSs form, and minima during the night - where MCS-produced moisture anomalies slowly diffuse to even out (Figure 1d). However, during this time interval, the daily average Var(PW) remains relatively constant for all simulations, even though it is already considerably larger for DIU. After day 14, DIU starts showing an increase in Var(PW) whereas OCEAN continues to show near-zero Var(PW). Repeating these simulations for two-fold higher and four-fold lower horizontal resolution shows qualitative similar results (Figure 2). One would expect the OCEAN lores, short for "low-resolution," simulation to aggregate due to its coarse horizontal resolution of 4 km and the domain of length 480 km, following C. J. Muller and Held (2012) and Yanase et al. (2020). However, albeit a certain monotonicity in the Var(PW) with respect to Δx, this simulation does not aggregate in the simulated time frame of 28 days, possibly due to the combination of chosen physics parameterization schemes and the suppression of top of atmosphere radiative cycles. We also note that we ran an OCEAN warm simulation, to highlight that even with a higher SST that matches the average SST in DIU, the OCEAN simulation does not aggregate in this time frame either (Figure 2).

Similar to Jensen et al. (2022), we mimic the land-sea transition of the deep convective cloud field, by branching off from the DIU simulation onto a constant SST (DIU2OCEAN). Here, however, we repeat the branching at different times of day (A: 6am, B: 12 noon, C: 6pm, D: 12am) and on different days of the simulation (days 14 and 28 (Figure 3). This allows us to study whether the diurnal phase of a branching—that is whenever a land-born

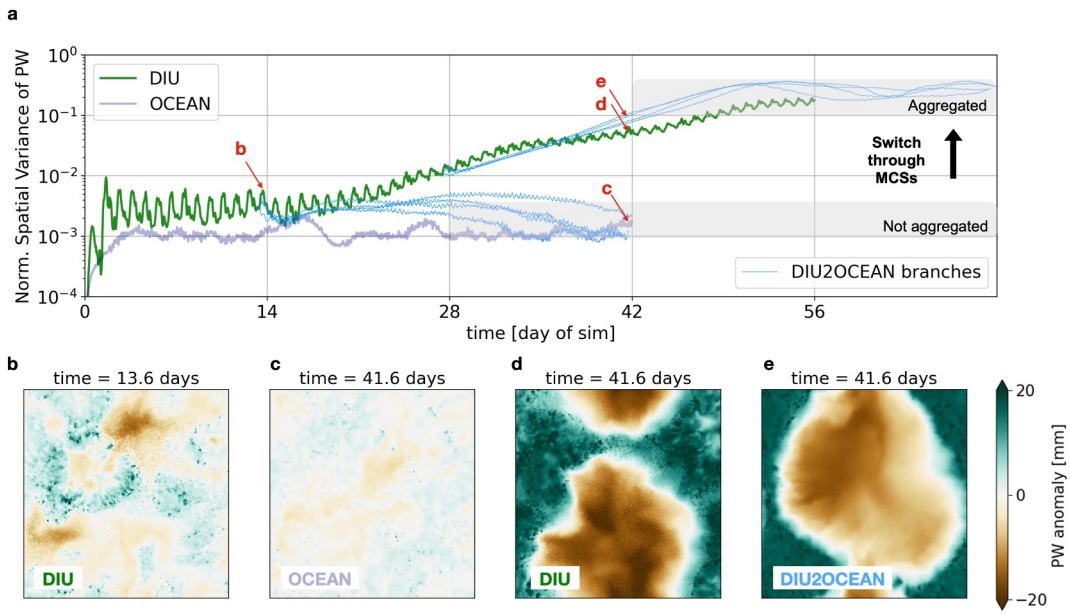

Figure 3. Bistable switching through mesoscale convective systems. Analogous to Figure 2, however now allowing for a branching off between DIU and OCEAN simulations. DIU2OCEAN branches originate near day 14 and day 28, respectively and are shown in light blue colors. OCEAN simulations without branching are shown in light purple colors (see legend). Steady-state regions of high and low normalized PW variance are indicated by light gray shades. Insets (b–e) exemplify the spatial pattern of PW anomalies at specific times of the simulation (see red arrows and panel labels for the exact timing). Note again the logarithmic vertical axis scaling.

MCS moves over the ocean—matters to its growth. Further, we also observe how MCS residence-time over land —akin to their "maturity"—matters to determine whether the system will aggregate over the ocean. The effects of land-sea transition appears clearly when comparing the branches initialized from DIU day 14 (branches DIU2OCEAN $A_1B_1C_1D_1$ in Table 1) to the branches initialized from DIU day 28 (branches DIU2OCEAN $A_2B_2C_2D_2$ in Table 1). Branches $A_1B_1C_1D_1$ fail to maintain the degree of aggregation already acquired in the DIU simulations (Figure 3) and their Var(PW) gradually returns to the values obtained by the original OCEAN simulation. Interestingly, the DIU2OCEAN D_1-branching (occurring at midnight) does appear to resist the change better than the other phases, suggesting that MCSs crossing the coastline at this time of the day have better chances of strengthening over the ocean. At midnight, in our DIU simulation, the surface temperature is 295 K. The transition to the warmer OCEAN SST of 300 K could favor, at least initially, the maintenance of the phase separation in the PW field, and thus a higher Var(PW). On the other hand, branches $A_2B_2C_2D_2$, proceed to aggregate further and even more rapidly than the continuation of DIU (Figure 3), reaching a fully aggregated state with characteristic low frequency fluctuations, similar to those seen and described in Patrizio and Randall (2019). This time, the time-of-transition appears not to the matter, and all trajectories behave similarly, suggesting that the MCS was already strong enough over the land to quickly dissipate over the ocean. Thus, we can conclude that the system shows bistability, with one low and one high spatial variance state. A transition between the low and the high variance state can be achieved by diurnal surface temperature forcing and the resultant MCS, but not through constant temperature lower boundary conditions.

The concept of bistability in CSA is not new (Bretherton et al., 2005; Craig & Mack, 2013; Emanuel et al., 2014; Shi & Fan, 2021; Sobel et al., 2007), however the dependance on the amplitude of the diurnal cycle in determining the bistability, appear first in Jensen et al. (2022). By employing a different CRM (SAM), in contrast to the UCLA-LES model used in their study, we similarly find that the diurnal cycle in surface temperature can induce persistent moisture patterns that profoundly impact on the multi-day precipitation distribution, thus adding additional robustness to the mechanism proposed in Jensen et al. (2022). On a time scale of hours, simply imposing a realistic diurnal cycle in the surface temperature of a CRM can produce large MCS-like deep convective structures during the afternoon hours. These structures do not develop within these time scales in simulations with constant surface temperature, which instead mimic the observed oceanic deep convection that

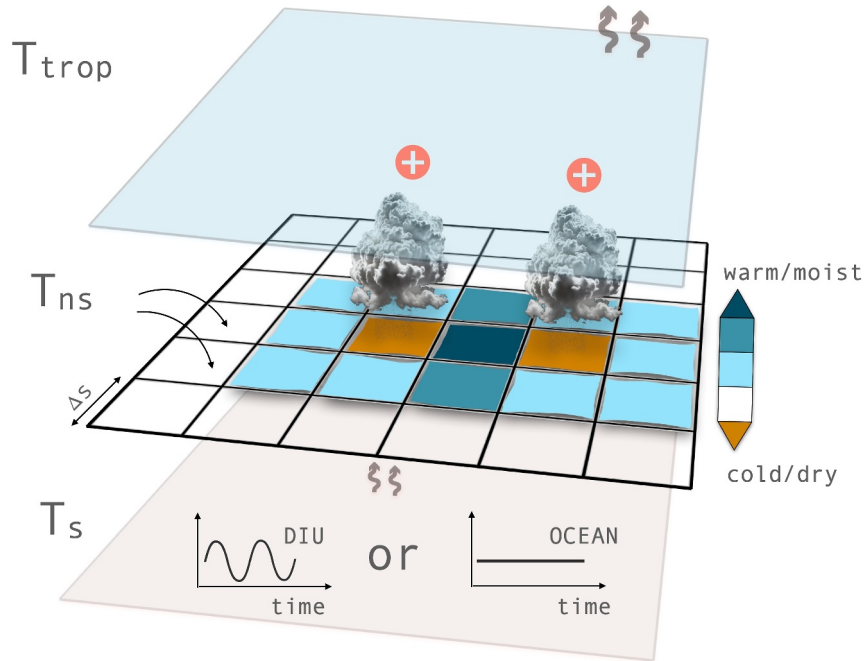

Figure 4. The Game of Cloud. Conceptual schematic of our model to study Convective Self-Aggregation developing from mesoscale convective systems. From bottom layer to the top: Surface temperature, T_s, is either prescribed as oscillating with a diurnal frequency (land) or constant (ocean); near-surface temperature, T_{ns}, is discretized on a 2D grid, where each grid cell assumes a value based on T_s, caused by surface heat fluxes, its neighbors, due to diffusion, and boundary-layer CP dynamics. Tropospheric temperature, T_{trop}, assumes one value for the entire troposphere. When $T_{ns} > T_{trop}$, deep convection can arise in the corresponding column, which triggers CP dynamics, decreasing T_{ns} beneath the rain cell and enhancing T_{ns} for its neighboring grid cells, and increasing T_{trop}. T_{trop} gradually cools at a set rate.

occurs irrespective of day and night and with smaller spatial extent. On a time scale of days, the land-like simulations furthermore develop a typical self-aggregated state in the moisture field, where parts of the domain become too dry to support any new convection, whereas such persistent drying does not develop at these timescales in the ocean-like simulations. Ocean-like simulations are able to maintain the aggregated moisture field, once this is sufficiently developed in land-like simulations. The fact that an earlier branching after 14 days does not yield persistent aggregation suggests that a substantial perturbation away from a linearly stable, homogeneous RCE state is needed.

Bringing our results into a realistic context, if we consider self-aggregation to be present to some extent in the real atmosphere, and land-produced MCSs to be a path to self-aggregation, then the residence time of a volume of atmosphere over land is an important factor in determining the maintenance of an aggregated state once it is advected over the ocean. This could mean that MCSs—produced over tropical African land—could be the key player needed in pushing the moisture distribution of the volume of atmosphere they are embedded within to an aggregated state, which might then be able to persist over the ocean—given that spatial moisture variance is high enough. This could be a so-far-missing ingredient for tropical cyclogenesis from the CSA point of view.

2.2. Conceptualizing the Bistability of Self-Aggregation

We implement a conceptual cellular automaton model, which we will call the "Game of Cloud," to study the basic physical mechanisms that can drive diurnal self-aggregation and the resulting hysteresis effect.

2.2.1. Conceptual Model Description

We demand that the model captures: (a) The spatial segregation effect which is seen in DIU but is absent in OCEAN; (b) long-term persistence for DIU; (c) the hysteresis effect described for the DIU2OCEAN branches; (d) realistic domain-mean diurnal cycles of convective rain. The model assumes three vertical layers and describes the dynamics of buoyancy in each of the three. We use the term "temperature" in the following to refer to an

appropriate measure of buoyancy for the moist atmosphere, such as entropy. We distinguish such temperature within (see also Figure 4): (a) The surface, which has a spatially-homogeneous and prescribed temperature $T_s(t)$ and is assumed to be at saturation, thus representing a water surface or a swamp. (b) The near-surface atmosphere temperature $T_{ns}(x,y,t)$, where we retain a horizontal spatial variation, as described further below; (c) the free-tropospheric temperature, which responds to $T_{ns}(x,y,t)$ but acts as a spatially equilibrated field $T_{trop}(t)$, such that it remains spatially-homogeneous.

Spatial and temporal discretization. The model uses for horizontal coordinate system (x,y), a uniformly-discretized square domain with periodic boundary conditions. A spatial resolution of $\Delta s \equiv 10$ km is chosen, which represents a typical spatial scale of isolated deep convective raincells and their individual CPs. Therefore, each discrete coordinate $(x,y) = (x_i,y_j)$ simply corresponds to the position $(x,y) = (i,j)\Delta s$, where i and j take integer values between 0 and $N-1$, where N is the number of pixels in each horizontal dimension. The near-surface temperature $T_{ns}(x,y,t)$ is defined at the discrete spatial coordinates described above. The typical temporal scale is assumed to be $\Delta t \equiv 30$min, representing the period between triggering of a given raincell and the initiation of the resultant rain event. Δt is both the characteristic time scale of convection, and the time step used in the discretization of the governing equations. For both model variables, T_{ns} and T_{trop}, the dynamics therefore evolve in discrete time steps of Δt, that is, each time point is defined as $k\Delta t$, where $k = 0,1,\ldots$ is an integer.

Boundary conditions. As explained before, the surface temperature, $T_s(t)$, is spatially homogeneous and prescribed as the harmonic function defined in Equation 1. It is represented in the bottom layer of the schematic in Figure 4. Importantly, $T_{trop}(t)$ is globally increased by any deep convective event—wherever it occurs—which is assumed to release a fixed quantity c_0 of latent heat of condensation (the plus signs in Figure 4). In fact in the real atmosphere, the positive buoyancy anomaly associated with a deep convective event is rapidly spread in the horizontal through the excitement of gravity waves. Further, the troposphere continuously cools under radiative emission at a constant rate $R \approx 3\text{K day}^{-1}$, as a simple approximation of the daily averaged tropospheric cooling that one could expect in the tropics (Fildier et al., 2023; Jeevanjee & Fueglistaler, 2020). The instantaneous rate of change of T_{trop} reads as:

$$\frac{dT_{trop}(t)}{dt} = C(t) - R, \tag{3}$$

where $C(t)$ would be the convective heat flux into the free troposphere at time t. In our discretized model dynamics, Equation 3 becomes

$$\Delta T_{trop} = nc_0 - R\Delta t. \tag{4}$$

Equation 4 is applied at every timestep Δt, and the integer n counts the number of convective events within the given timestep. It is assumed that the horizontal domain size is small enough such that the weak temperature gradient approximation applies (Sobel et al., 2001), thus justifying the assumption of a spatially homogeneous field $T_{trop}(t)$.

Near surface conditions and diffusivity. For the near-surface atmospheric (virtual) temperature, $T_{ns}(x,y,t)$, the continuum version of the basic model dynamics can be summarized as a prognostic equation, namely.

$$\frac{d}{dt}T_{ns}(x,y,t) = \underbrace{\frac{1}{\tau}(T_s(t) - T_{ns}(x,y,t))}_{\text{surface-atmosphere heat flux}} + \underbrace{D_h\nabla^2 T_{ns}(x,y,t)}_{\text{horizontal diffusion}} \tag{5}$$

$$+ \underbrace{\mathcal{R}(x,y,t;\{x_i\},\{y_j\},\{t_l\})}_{\text{reactive processes}} \tag{6}$$

$$+ \underbrace{b_1\, T'_{ns}(x,y,t)\left(1 - b_2 T'^2_{ns}(x,y,t)\right)}_{\text{moisture-radiation-circulation feedback}}, \tag{7}$$

In Equation 7, $T'_{ns}(x,y,t) \equiv T_{ns}(x,y,t) - \overline{T_{ns}}(t)$, with $\overline{T_{ns}}(t)$ the spatial mean of $T_{ns}(x,y,t)$ at time t. The surface-atmosphere heat flux is a diffusive flux generated by the temperature difference between the surface and the atmosphere, and modulated by the time scale τ. The $T_{ns}(x,y,t=0)$ field is initialized with random noise, to initiate the first convection. Wind speed effects on surface-atmosphere heat fluxes are neglected for simplicity. The horizontal diffusion is implemented to capture all horizontal mixing processes taking place through eddy-diffusive motion within the boundary layer.

Positive feedback mechanism. The term in Equation 7 describes a moisture-radiation-circulation feedback, mimicking the "rich-gets-richer" dynamics invoked in previous works on CSA (Bretherton et al., 2005; C. Muller et al., 2022; Wing et al., 2017). In effect, the resultant action of sustained subsidence is to dry the near-surface atmosphere, thus leading to further drying in regions that are already dry. Conversely, we allow moist regions to moisten further. The positive coefficients b_1 and b_2 in Equation 7 prohibit unbounded decrease or increase of buoyancy, thus ensuring a naturally occurring maximum or minimum in buoyancy. Specifically, the $1 - b_2 T'^2_{ns}$ factor ensures that while small perturbations in T'_{ns} initially grow or decay exponentially, this growth is suppressed as T'_{ns} becomes large, preventing unrealistic extremes. This formulation accounts for physical constraints that prevent arbitrarily extreme temperatures, such as strong Stefan-Boltzmann thermal emission or other stabilizing mechanisms. In our cellular automaton model Equations 5–7 are discretized in spatial and temporal steps of Δs and Δt to match the typical convective scales assumed.

Triggering of convection. We now turn to the reactive term $\mathcal{R}$ Equation 6, which introduces a measure of stochasticity into the model. $\mathcal{R}\left(x,y,t;\{x_i\},\{y_j\},t\right)$ models the threshold-like triggering of a convective event at any discrete location (x,y) at time t. The reactive term consists of two parts of which the first allows individual locations (x,y) to interact with other locations through the "mean field" $T_{trop}(t)$: during a given timestep Δt, all locations (x,y) with $T_{ns}(x,y,t) > T_{trop}(t)$ are considered potentially unstable. To each of these locations (x,y) we therefore assign a triggering probability

$$p(x,y,t) \propto T_{ns}(x,y,t) - T_{trop}(t) > 0, \tag{8}$$

which assumes that locations with buoyancy exceeding that of the free troposphere may be unstable to convection. In a random procedure, we now sequentially draw locations from the list of unstable locations according to their probabilities $p(x,y,t)$ and for each of them transfer condensation heat c_0 to the free troposphere, thus, for each of them, increasing $T_{trop}(t)$. We therefore then update all $p(x,y,t)$ as the increase in $T_{trop}(t)$ will often have stabilized a number of the previously unstable locations. During the given timestep this stochastic procedure is repeated until all locations are stable.

The second part of $\mathcal{R}$ models the suppression and activation of new convective raincells through CPs. Cold pool effects are incorporated in a two-fold manner, reflecting known physical processes: at each timestep t, the temperature $T_{ns}(x,y,t)$ at any given location (x,y) which was occupied by raincells at time $t - \Delta t$ is lowered by ΔT_{cp}, mimicking the well-known near-surface evaporative cooling experienced beneath deep convective clouds. Further, to mimic thermodynamic and mechanical triggering at the edges of existing CPs, such as by forced lifting or collision effects, the $T_{ns}(x,y,t)$ at any such location (x,y) is incremented by a term that is proportional to the number of surrounding locations that had active rainfall at $t - \Delta t$, where the 8-neighborhood of the location (x,y) is used to define the neighborhood. This weighting ensures that locations surrounded by one or several CPs are more likely to experience convective triggering. We note here that a rainy pixel is considered "active" for two time steps, that is, 1 hour, to increase the chance of nearby raincells to interact with each other.

In a cellular automaton step, denoted by an arrow below, a temperature enhancement is applied specifically to any pixel (x,y) that is inactive (not raining) at time t as:

$$T_{ns}(x,y,t) \rightarrow T_{ns}(x,y,t) + I\,|\Delta T_{cp}|\,\overline{T}_{ns}(t) \cdot n/8 \tag{9}$$

where n is the number of active neighbors of the pixel (x,y) at time t and I is a coefficient that scales the magnitude of the triggering of new convection. The proportionality with $\overline{T}_{ns}(t)$ ensures that the triggering effect does not dominate when $\overline{T}_{ns}(t)$ is low, such as at night for DIU, or generally for OCEAN, and the proportionality with ΔT_{cp} ensures that the triggering effect is stronger (weaker) for strong (weak) CPs when changing ΔT_{cp} (as in Figure 7).

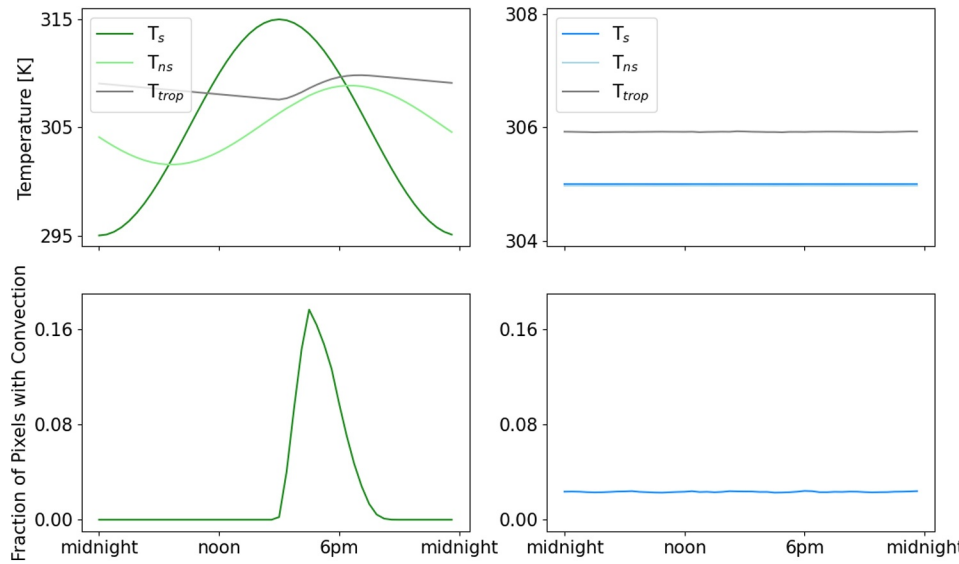

Figure 5. Diurnal time series in the Game of Cloud. (a), Diurnal cycle of temperatures T_s, T_{ns} and T_{trop} for the DIU configuration. (b), as (a) but for OCEAN. Note that $T_{ns} = T_s = 305$ K here. (c, d), Convective precipitation diurnal cycle for DIU and OCEAN, respectively.

2.2.2. Conceptual Model Properties

With the parameters chosen (Table 2), our model captures the mean diurnal cycle of convection of land and sea (Figure 5) by imposing $\Delta T = 10$ K for land and $T_0 = 305$ K for land and ocean. We compute the normalized spatial variance of T_{ns} (Figure 6), which shows constantly small values throughout the timeseries for the $\Delta T = 0$ case, whereas $\Delta T = 10$ K yields a systematic increase over the course of 28 days and subsequent saturation. When switching to $\Delta T = 0$ after 28 days of $\Delta T = 10$ K, our model also shows that variance is preserved, thus capturing the hysteresis effect. Examining spatial patterns at day 42 reveals that T_{ns} is structured into mesoscale clusters for the diurnally oscillating case, whereas T_{ns} remains scattered for the constant-T_s counterpart.

Qualitatively, the conceptual model dynamics compares well to the variance of PW for the SAM simulations, as the spatial segregation effect seen in DIU but not in OCEAN is reproduced, long-term persistence for DIU is captured and the hysteresis effect described for the DIU2OCEAN branches is mimicked. Furthermore, the diurnal cycles of convective rain are realistic (Figure 5).

2.2.3. Parametric Sensitivity Study

In an effort to better illustrate the model's driving mechanisms, a parametric study is carried out within the $(\Delta T, \Delta T_{CP}, D_h)$-space, limits of which are defined by the axes in Figure 7. As a reminder, these parameters respectively quantify (a) the diurnal cycle amplitude—which determines the surface temperature forcing regime (DIU/OCEAN)—and (b) the CP cooling strength and (c) the rate at which horizontal temperature is homogenized. These parameters are varied sequentially two-by-two while the third one retains its default value, as presented in Table 2. The parametric space was chosen as wide as possible while retaining physically-relevant bounds. Further, each parameter was varied 50 times, resulting in a total of 7,500 configurations, which all ran for 100 model days. Finally, over the course of these 100 days, two metrics were evaluated to quantify the model's response to a particular $(\Delta T, \Delta T_{CP}, D_h)$-solution: (a) The spatial variance of T_{ns} on day 100 and (b) the day when this quantity reached a threshold of 0.05.

The resulting contour maps are presented in Figure 7, with the default values represented with dashed red lines. The OCEAN configuration is marked by a dashed blue line, while the DIU configuration studied above is marked by a green dashed line.

Diurnal amplitude ΔT. An increase in ΔT consistently enhances both CSA metrics (Figures 7a–7d): Large ΔT overcomes the anti-aggregating dynamics caused by a high horizontal diffusion or strong CPs. A ΔT_{CP} of 1.5 K

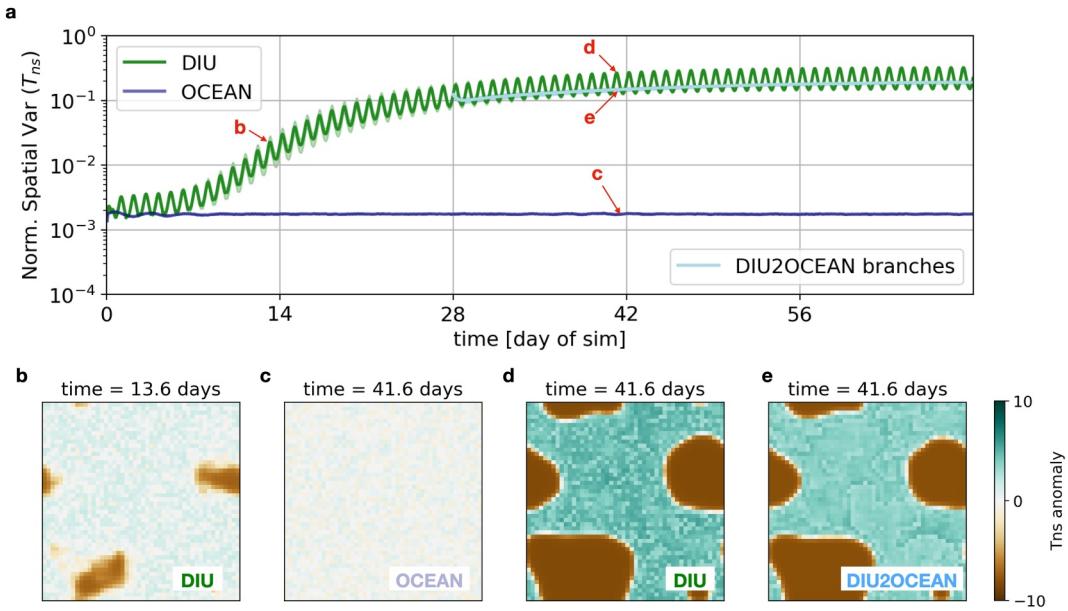

Figure 6. Bistable switching through mesoscale convective systems in the Game of Cloud. Conceptual model analog of Figure 3 showing the normalized spatial variance of near surface temperature, T_{ns}, for DIU, OCEAN and DIU2OCEAN branches originating near day 28. Light shading indicates spread over 10 simulations. Insets (b–e) show the spatial pattern for specific times and simulations. Note again the logarithmic vertical axis scaling.

can consistently prevent aggregation until the diurnal cycle amplitude reaches about 6 K, at which point it seems to be the dominating organizational driver (Figure 7d). This is consistent with findings from Jensen et al. (2022), where strong surface temperature amplitude would trigger convective aggregation. Importantly, the ($\Delta T = 0$)-case—corresponding to OCEAN—is still capable of aggregating under specific circumstances, such as *weak* CPs (i.e., low ΔT_{CP}) or little horizontal diffusion (i.e., low D_h). This captures findings from a range of RCE simulations that aggregate with temporally uniform SST (Wing et al., 2017).

Cold pool cooling strength ΔT_{CP}. Strikingly, $\Delta T_{CP} = 0$ K—corresponding to no CP dynamics—invariably leads to aggregation, regardless of the other parameter values. The de-aggregating force of CPs is consistent

Table 2
Parameters Used in the Game of Cloud

Symbol	Numerical value	Notes
Δs	10 km	spatial scale of individual deep convective events
N	50	linear dimension in units of Δs (grid size)
Δt	30 min	time step approximating a convective life cycle
ΔT	10 K	diurnal surface temperature amplitude
ΔT_{cp}	−2 K	cooling induced by a CP
D_h	100 m^2 s^{-1}	horizontal eddy-diffusion coefficient
τ	10 hours	surface-atmosphere heat diffusion time scale
I	0.7 K^{-1}	scaling coefficient for CP triggering of convection
b_1	0.06 s^{-1}	moisture-radiation feedback coefficient 1
b_2	1 K^{-2}	moisture-radiation feedback coefficient 2
c_0	4 N^{-2} K	tropospheric heating due to a single convective event
R	3 K day^{-1}	free tropospheric diurnal cooling rate

Note. Table indicates the parameters used in the conceptual model, including the mathematical symbol, the numerical value and notes on the respective physical meaning.

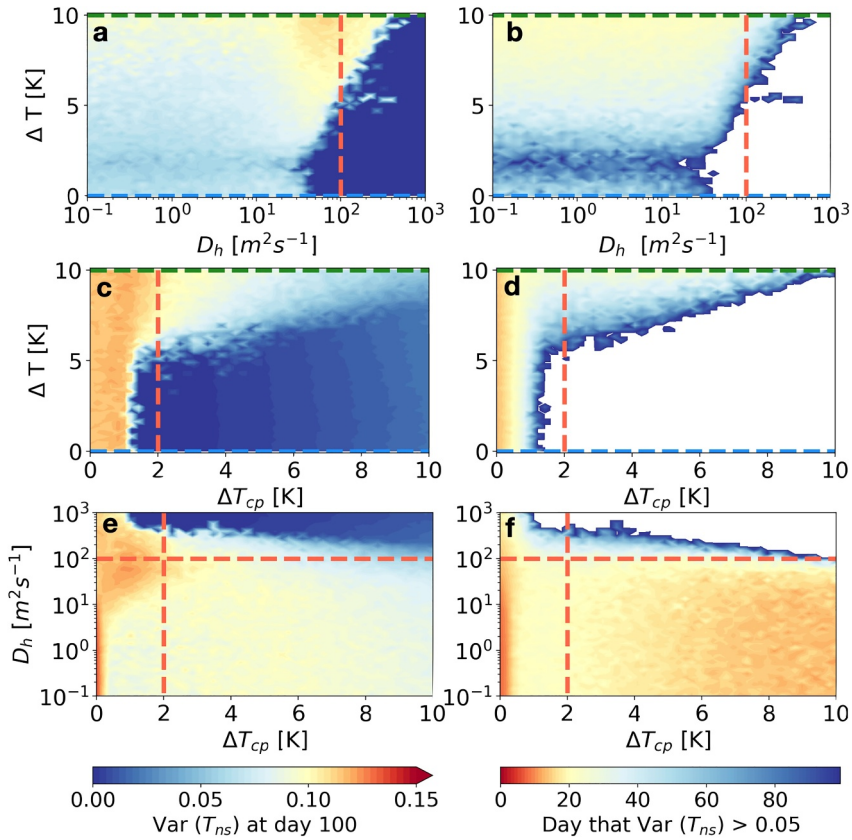

Figure 7. Exploring the parameter space of the Game of Cloud. Left column indicates the level of aggregation (measured by spatial variance of T_{ns}) as a function of parameter space after 100 days of simulation. Right column indicates day of the simulation that the level of aggregation has surpassed the value of 0.05. The parameter space explored comprises the diurnal cycle amplitude ΔT, cold pool strength ΔT_{CP} and horizontal diffusion D_h. Green dashed lines indicate the chosen ΔT for DIU, blue dashed lines indicate the chosen ΔT for OCEAN, red dashed lines indicate the chosen parameters for ΔT_{CP} and D_h in our default runs.

with the observation from idealized RCE studies (Jeevanjee & Romps, 2013; C. Muller & Bony, 2015; Nissen & Haerter, 2021) where disabling rain evaporation in the lower levels - thereby removing CPs—enhanced CSA. Conversely, increasing ΔT_{CP} progressively overwhelms the other parameters' importance, suggesting that the de-aggregating force increases with CP strength. This is also consistent with the work of Meyer and Haerter (2020), who observed how both the size and propagating velocity of CPs increases with the initial temperature reduction. Interestingly, stronger CPs may speed up aggregation at low horizontal eddy diffusivity and in the presence of a diurnal cycle (Figure 7f). This, again, echoes the recent work of Jensen et al. (2022) who observed numerically how strong *macro*-cold pools could contribute to a form of self-aggregation by forming persistently dry regions.

Horizontal eddy diffusivity $\mathbf{D_h}$. Strong horizontal diffusion is capable of completely shutting down aggregation through brute-force damping of any spatial heterogeneities (Figures 7a, 7b, 7e, and 7f). Overall, our model's response to enhanced D_h is similar to that of Biagioli and Tompkins (2023), for the evolution of column-integrated relative humidity. They also observe that horizontal diffusivity acts to counter-balance CSA by redistributing moisture away from rainy clusters into dry regions.

In summary, the model is shown to behave consistently with more complex and idealized studies of CSA. However, we note that all our simulations are deliberately idealized, to reveal the key mechanisms involved in the hysteresis-like effect of induced self-aggregation by the diurnal forcing. Important factors, such as wind shear, the Coriolis force, two-way coupling to the land or water surface, as well as topographic forcing and land-sea breezes, are left out and should be explored in follow-up work.

3. Conclusion

We have simulated tropical land-like MCSs by incorporating a realistic diurnal cycle amplitude in surface temperatures within a CRM, and we mimic the transition to the ocean by removing the diurnal cycle for ocean-like deep convection. Our results suggest that the diurnal cycle in surface temperature can induce persistent moisture patterns that profoundly impact the multi-day precipitation distribution, through the presence of MCSs, consistent with the recent literature (Jensen et al., 2022). On a time scale of hours, simply imposing a realistic diurnal cycle in the surface temperature of a CRM can produce large MCS-like deep convective structures during the afternoon hours. These structures do not develop under constant surface temperature conditions, mimicking oceanic deep convection that occurs irrespective of day and night and has smaller spatial extent. On a time scale of days, the land-like simulations furthermore develop a typical self-aggregated state where parts of the domain become too dry to support any new convection, whereas such persistent drying does not develop at these timescales in the ocean-like simulations.

Expanding on the finding of hysteresis in cloud resolving simulations transitioning from a diurnal cycle to none (Jensen et al., 2022) we here explore branching from the land-like to ocean-like simulations at different days and find that ocean-like simulations are able to maintain the aggregated moisture field only once this has reached a certain level of aggregation. To deepen our understanding of the key processes acting in these simulations, we develop a discrete reaction-diffusion-type model, characterized by three key parameters: the diurnal cycle amplitude, CP strength, and horizontal diffusion. The "Game of Cloud" model successfully captures the bistability observed in the transition from dispersed to aggregated states, demonstrating how diurnal temperature variations can drive spatial segregation in near-surface temperatures, leading to the formation of mesoscale convective clusters, while constant temperatures result in a more scattered spatial pattern. This segregation is persistent over time, even when diurnal variations cease, highlighting a hysteresis effect. The parametric sensitivity study further reveals that increasing the diurnal temperature amplitude (ΔT) enhances CSA, even in the presence of anti-aggregating forces like strong CPs or high horizontal diffusion. The findings align well with prior research, suggesting that both strong diurnal forcing and boundary layer dynamics are crucial for triggering and sustaining CSA in the atmosphere.

We conclude that MCSs over tropical land can induce domain-wide CSA within weeks, persisting even under ocean-like conditions where aggregation typically would not occur on such timescales. The "tipping" toward an aggregated state is, in other words, driven by diurnal cycle-induced MCSs. To illustrate this, we propose a regime diagram (Figures 8a and 8b) which represents a qualitative analogy to a dynamical system within a potential energy field V. Two stable equilibria are shown: The "Not aggregated" and "Aggregated" states, which can be identified by proxies like low and high spatial variance of PW as used in this study, or zero and nonzero mesoscale vertical velocity w to compare with previous work (Emanuel et al., 2014). In a linearly stable regime (Figure 8a), at low SSTs, w must be significantly displaced from its locally stable equilibrium $w = 0$ to reach a global minimum at nonzero w. However, at higher SSTs, even small perturbations can drive w to a stable nonzero equilibrium (Figure 8b). We view the diurnal cycle amplitude ΔT as a strong perturbation to the neutral state of $w = 0$, with sufficiently large ΔT disrupting symmetry and inducing a transition to nonzero w, which can then stabilize even if ΔT is removed. Thus, in low-SST conditions (Figure 8a), the "Not aggregated" state is a local equilibrium typical of standard RCE over tropical oceans, while the "Aggregated" state is the global equilibrium state for high perturbative ΔT, such as over tropical land—and once this global equilibrium is reached, it cannot easily be left. In other words, the ball in Figure 8a can be transported from the "Not aggregated" equilibrium to the "Aggregated" state via the action of MCSs that can help overcome the barrier. This can be compared to the seminal model by Emanuel et al. (2014), where CSA emerges from a linearly stable regime that destabilizes at higher SSTs (Figure 8c), leading to a structured state with distinct convecting and subsiding regions. Our results suggest that while the model remains linearly stable at low SSTs, diurnally-induced mesoscale organization can still drive a transition to a persistently organized state, with boundary layer moisture dynamics playing a crucial role in this process.

While we suggest that land-produced MCSs are the process by which a tropical atmospheric volume can "tip" to an aggregated state, the present work still leaves open which exact process within MCSs determines the emergence of persistent drying—and thus CSA. Haerter et al. (2020) suggested that so called "diurnal self-aggregation" occurs with a large enough diurnal cycle in surface temperature, due to the higher spatial density of rain cells within a short time window during the diurnal cycle, leading to the merging of convective CPs and the

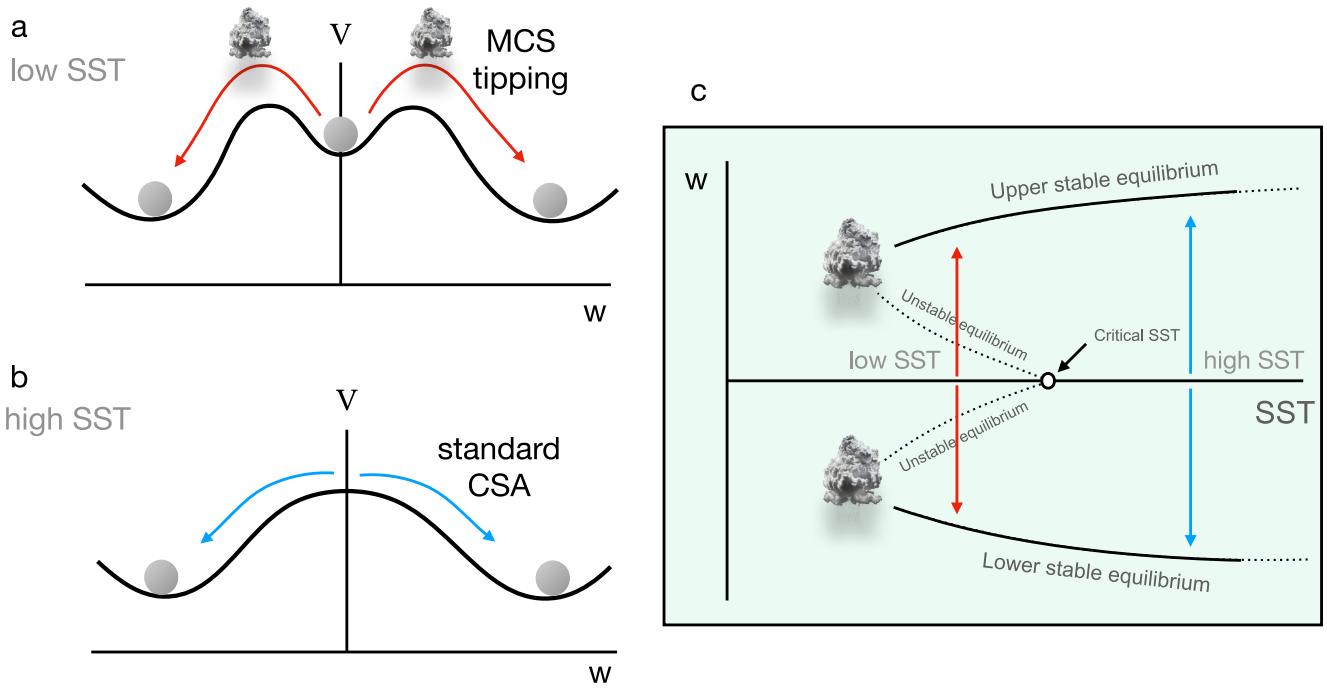

Figure 8. Transitions at low and high sea surface temperature (SST) as departures from stable and unstable equilibria. (a) Schematic regime diagram for the equilibrium state within the low SST regime. Mesoscale vertical velocity $w = 0$ ("Not aggregated" state) thereby constitutes a linearly stable equilibrium. The schematic should be viewed as an intuitive analogy to a particle in a potential energy landscape (V, vertical axis), that is, a dynamical system in a linearly stable regime. Clouds illustrate the system being "tipped" toward a $w \neq 0$ state ("Aggregated" state) by the dynamics of diurnal cycle-induced mesoscale convective systems. (b) Analogous to (a) but within the high SST regime. Note that the equilibrium is now linearly unstable to small perturbations in w. (c) Modified from Figure 7 in (Emanuel et al., 2014) with red and blue arrows suggesting how transitions relate to panels (a, b).

formation of a super CP. This larger CP triggers a cascade of convective rain cells along its gust front, contributing to the merged CPs, whose thermodynamic anomalies dissipate slowly, subsequently suppressing further convection in the same region on subsequent days, creating large dry areas that shut off convection and kick starting the positive radiative feedback mechanism driven by clear-sky effects in these dry areas. An alternative explanation could be that there is large subsidence around an MCS, which could, in principle, also create a large dry area that could first form in the higher levels of the troposphere, as seen in Jensen et al. (2022), then extend to the full atmospheric column and kickstart the same radiative feedback.

In either case, the origin of CSA would be intimately tied to the presence of MCSs. Yet, as we cannot pinpoint the cause of the "first dry region" in our simulations, we suggest this aspect to be explored further. Assuming that CPs of MCSs over land initially contribute to *accelerating* the onset of CSA, we point out that once the system is aggregated, these MCS-scale CPs act to redistribute moisture and *oppose* the radiative feedback over land by counteracting the radiative dry pool in the boundary layer (Yanase et al., 2020) and slow down self-aggregation. When the aggregated state then transitions to constant SSTs mimicking an ocean surface, the disappearance of MCSs replaced by isolated deep convection and their associated small CPs, cannot counteract the radiative dry pool—so at this stage the small sparse CPs are not an obstacle to aggregation at all. This is an explanation to the slowdown of the DIU curve in Figure 3 as opposed to the DIU2OCEAN branches, after about 6 weeks of simulation. The dual effect of CPs based on their size is not included in our conceptual model and could be further explored.

Follow-up work could include incorporating an easterly flow and wind-shear, to explore the effect of realistic wind profiles on the self-aggregated state transitioning from land to sea. A complementary observational study to ours could also be explored, to detect the footprint of CSA (as in high variance of PW, or large dry areas in the upper troposphere) around MCSs created over land, to see if these exist and if they persist when advected westward.

Our CRM simulations as well as the conceptual model suggest that land-produced MCSs can be a path to self-aggregation and that the residence time of a volume of atmosphere over land is crucial in determining the maintenance of an aggregated state once it is advected over the ocean. Mesoscale convective systems—produced over tropical African land—may thus carry the moisture feedback mechanisms needed in eventually yielding an aggregated state which might then be able to persist over the ocean, given that spatial moisture variance is high enough. In contrast to the classical CSA mechanisms alone, where the process of full aggregation is rather slow, MCS-based aggregation may be the missing ingredient for more speedy tropical cyclogenesis.

Data Availability Statement

ERA5 Reanalysis data was retrieved from the Copernicus Climate Change Service (C3S) Climate Data Store (CDS) (Hersbach et al., 2023). TOOCAN MCS tracks were retrieved from the TOOCAN database (TOOCAN Database, 2019) - the authors acknowledge the data center ESPRI/IPSL for providing access to the data. The modified SAM source code used for this study, along with parameter namelists for re-running the simulations, and codes for data analysis are available on Github (Kruse, 2024a). Source code for the Game of Cloud is available on Github (Kruse, 2024b). Statistical output from 4 main SAM CRM simulations in this study are available for download on Zenodo (Kruse, 2024c).

Acknowledgments

ILK would like to acknowledge Cristian Vraciu for insightful discussions on the Game of Cloud. The authors wish to thank three anonymous reviewers whose comments greatly contributed to the quality of this manuscript. The authors gratefully acknowledge funding by a grant from the VILLUM Foundation (Grant 13168) and the European Research Council (ERC) under the European Union's Horizon 2020 research and innovation program (Grant 771859) and the Novo Nordisk Foundation Interdisciplinary Synergy Program (Grant NNF19OC0057374). This work used resources of the Deutsches Klimarechenzentrum (DKRZ), granted by its Scientific Steering Committee (WLA) under project ID bb1166. Open Access funding enabled and organized by Projekt DEAL.

References

Biagioli, G., & Tompkins, A. M. (2023). A dimensionless parameter for predicting convective self-aggregation onset in a stochastic reaction-diffusion model of tropical radiative-convective equilibrium. *Journal of Advances in Modeling Earth Systems*, *15*(5), e2022MS003231. https://doi.org/10.1029/2022MS003231

Bretherton, C. S., Blossey, P. N., & Khairoutdinov, M. (2005). An energy-balance analysis of deep convective self-aggregation above uniform sst. *Journal of the Atmospheric Sciences*, *62*(12), 4273–4292. https://doi.org/10.1175/jas3614.1

Craig, G. C., & Mack, J. M. (2013). A coarsening model for self-organization of tropical convection. *Journal of Geophysical Research: Atmospheres*, *118*(16), 8761–8769. https://doi.org/10.1002/jgrd.50674

Emanuel, K., Wing, A. A., & Vincent, E. M. (2014). Radiative-convective instability. *Journal of Advances in Modeling Earth Systems*, *6*(1), 75–90. https://doi.org/10.1002/2013MS000270

Fang, J., & Du, Y. (2022). A global survey of diurnal offshore propagation of rainfall. *Nature Communications*, *13*(1), 7437. https://doi.org/10.1038/s41467-022-34842-0

Fildier, B., Muller, C., Pincus, R., & Fueglistaler, S. (2023). How moisture shapes low-level radiative cooling in subsidence regimes. *AGU Advances*, *4*(3), e2023AV000880. https://doi.org/10.1029/2023AV000880

Fiolleau, T., & Roca, R. (2013). An algorithm for the detection and tracking of tropical mesoscale convective systems using infrared images from geostationary satellite. *IEEE Transactions on Geoscience and Remote Sensing*, *51*(7), 4302–4315. https://doi.org/10.1109/TGRS.2012.2227762

Haerter, J. O., Meyer, B., & Nissen, S. B. (2020). Diurnal self-aggregation. *npj Climate and Atmospheric Science*, *3*(1), 1–11. https://doi.org/10.1038/s41612-020-00132-z

Held, I. M., Hemler, R. S., & Ramaswamy, V. (1993). Radiative-convective equilibrium with explicit two-dimensional moist convection. *Journal of the Atmospheric Sciences*, *50*(23), 3909–3927. https://doi.org/10.1175/1520-0469(1993)050⟨3909:RCEWET⟩2.0.CO;2

Hersbach, H., Bell, B., Berrisford, P., Biavati, G., Horányi, A., Muñoz Sabater, J., et al. (2023). ERA5 hourly data on single levels from 1940 to present. *Copernicus Climate Change Service (C3S) Climate Data Store (CDS)*. https://doi.org/10.24381/cds.adbb2d47

Holloway, C. E., Wing, A. A., Bony, S., Muller, C., Masunaga, H., L'Ecuyer, T. S., et al. (2017). Observing convective aggregation. *Surveys in Geophysics*, *38*(6), 1199–1236. https://doi.org/10.1007/s10712-017-9419-1

Houze, R. A. (2018). 100 years of research on mesoscale convective systems. *Meteorological Monographs*, *59*(1), 17.1–17.54. https://doi.org/10.1175/AMSMONOGRAPHS-D-18-0001.1

Jeevanjee, N., & Fueglistaler, S. (2020). Simple spectral models for atmospheric radiative cooling. *Journal of the Atmospheric Sciences*, *77*(2), 479–497. https://doi.org/10.1175/JAS-D-18-0347.1

Jeevanjee, N., & Romps, D. M. (2013). Convective self-aggregation, cold pools, and domain size. *Geophysical Research Letters*, *40*(5), 994–998. https://doi.org/10.1002/grl.50204

Jensen, G. G., Fiévet, R., & Haerter, J. O. (2022). The diurnal path to persistent convective self-aggregation. *Journal of Advances in Modeling Earth Systems*, *14*(5), e2021MS002923. https://doi.org/10.1029/2021MS002923

Khairoutdinov, M. F., & Emanuel, K. (2010). Aggregated convection and the regulation of tropical climate. In *29th Conf. on Hurricanes and Tropical Meteorology*. American Meteorological Society.

Khairoutdinov, M. F., & Randall, D. A. (2003). Cloud resolving modeling of the arm summer 1997 iop: Model formulation, results, uncertainties, and sensitivities. *Journal of the Atmospheric Sciences*, *60*(4), 607–625. https://doi.org/10.1175/1520-0469(2003)060⟨0607:CRMOTA⟩2.0.CO;2

Kruse, I. L. (2024a). Code for tipping to an aggregated state by mesoscale convective systems. *Zenodo*. https://doi.org/10.5281/zenodo.13736017

Kruse, I. L. (2024b). Game of cloud. *Zenodo*. https://doi.org/10.5281/zenodo.13735995

Kruse, I. L. (2024c). Post-processed SAM (system for atmospheric modeling) simulation output for tipping to an aggregated state by mesoscale convective systems. *Zenodo*. https://doi.org/10.5281/zenodo.13622727

Meyer, B., & Haerter, J. O. (2020). Mechanical forcing of convection by cold pools: Collisions and energy scaling. *Journal of Advances in Modeling Earth Systems*, *12*(11), e2020MS002281. https://doi.org/10.1029/2020ms002281

Muller, C., & Bony, S. (2015). What favors convective aggregation and why? *Geophysical Research Letters*, *42*(13), 5626–5634. https://doi.org/10.1002/2015GL064260

Muller, C., Yang, D., Craig, G., Cronin, T., Fildier, B., Haerter, J. O., et al. (2022). Spontaneous aggregation of convective storms. *Annual Review of Fluid Mechanics*, *54*(1), null–157. https://doi.org/10.1146/annurev-fluid-022421-011319

Muller, C. J., & Held, I. M. (2012). Detailed investigation of the self-aggregation of convection in cloud-resolving simulations. *Journal of the Atmospheric Sciences*, *69*(8), 2551–2565. https://doi.org/10.1175/jas-d-11-0257.1

Nesbitt, S. W., Zipser, E. J., & Cecil, D. J. (2000). A census of precipitation features in the tropics using trmm: Radar, ice scattering, and lightning observations. *Journal of Climate*, *13*(23), 4087–4106. https://doi.org/10.1175/1520-0442(2000)013⟨4087:ACOPFI⟩2.0.CO;2

Nissen, S. B., & Haerter, J. O. (2021). Circling in on convective self-aggregation. *Journal of Geophysical Research: Atmospheres*, *126*(20), e2021JD035331. https://doi.org/10.1029/2021jd035331

Oliver, J. E. (2005). Bowen ratio. In J. E. Oliver (Ed.), *Encyclopedia of world climatology* (pp. 178–179). Dordrecht: Springer Netherlands. https://doi.org/10.1007/1-4020-3266-8_33

Patrizio, C. R., & Randall, D. A. (2019). Sensitivity of convective self-aggregation to domain size. *Journal of Advances in Modeling Earth Systems*, *11*(7), 1995–2019. https://doi.org/10.1029/2019MS001672

Roca, R., & Fiolleau, T. (2020). Extreme precipitation in the tropics is closely associated with long-lived convective systems. *Communications Earth & Environment*, *1*(1), 1–6. https://doi.org/10.1038/s43247-020-00015-4

Rotunno, R., Klemp, J. B., & Weisman, M. L. (1988). A theory for strong, long-lived squall lines. *Journal of the Atmospheric Sciences*, *45*(3), 463–485. https://doi.org/10.1175/1520-0469(1988)045⟨0463:ATFSLL⟩2.0.CO;2

Shi, X., & Fan, Y. (2021). Modulation of the bifurcation in radiative-convective equilibrium by gray-zone cloud and turbulence parameterizations. *Journal of Advances in Modeling Earth Systems*, *13*(10), e2021MS002632. https://doi.org/10.1029/2021MS002632

Sobel, A. H., Bellon, G., & Bacmeister, J. (2007). Multiple equilibria in a single-column model of the tropical atmosphere. *Geophysical Research Letters*, *34*(22). https://doi.org/10.1029/2007GL031320

Sobel, A. H., Nilsson, J., & Polvani, L. M. (2001). The weak temperature gradient approximation and balanced tropical moisture waves. *Journal of the Atmospheric Sciences*, *58*(23), 3650–3665. https://doi.org/10.1175/1520-0469(2001)058<3650:twtgaa>2.0.co;2

Tan, J., Jakob, C., Rossow, W. B., & Tselioudis, G. (2015). Increases in tropical rainfall driven by changes in frequency of organized deep convection. *Nature*, *519*(7544), 451–454. https://doi.org/10.1038/nature14339

Tompkins, A. M. (2001). Organization of tropical convection in low vertical wind shears: The role of cold pools. *Journal of the Atmospheric Sciences*, *58*(13), 1650–1672. https://doi.org/10.1175/1520-0469(2001)058⟨1650:OOTCIL⟩2.0.CO;2

Tompkins, A. M., & Craig, G. C. (1998). Radiative–convective equilibrium in a three-dimensional cloud-ensemble model. *Quarterly Journal of the Royal Meteorological Society*, *124*(550), 2073–2097. https://doi.org/10.1002/qj.49712455013

TOOCAN Database. (2019). ESPRI/IPSL data center. https://doi.org/10.14768/20191112001.1

Torri, G., Kuang, Z., & Tian, Y. (2015). Mechanisms for convection triggering by cold pools. *Geophysical Research Letters*, *42*(6), 1943–1950. https://doi.org/10.1002/2015GL063227

Wing, A. A., Emanuel, K., Holloway, C. E., & Muller, C. (2017). Convective self-aggregation in numerical simulations: A review. *Surveys in Geophysics*, *38*, 1173–1197. https://doi.org/10.1007/s10712-017-9408-4

Yanase, T., Nishizawa, S., Miura, H., Takemi, T., & Tomita, H. (2020). New critical length for the onset of self-aggregation of moist convection. *Geophysical Research Letters*, *47*(16), e2020GL088763. https://doi.org/10.1029/2020GL088763

Zipser, E. J., Cecil, D. J., Liu, C., Nesbitt, S. W., & Yorty, D. P. (2006). Where are the most intense thunderstorms on earth? *Bulletin of the American Meteorological Society*, *87*(8), 1057–1072. https://doi.org/10.1175/BAMS-87-8-1057